NANO · MICRO small
www.small-journal.com

Pair Interaction between Two Catalytically Active Colloids

Priyanka Sharan, Abdallah Daddi-Moussa-Ider, Jaime Agudo-Canalejo, Ramin Golestanian, and Juliane Simmchen**

Due to the intrinsically complex non-equilibrium behavior of the constituents of active matter systems, a comprehensive understanding of their collective properties is a challenge that requires systematic bottom–up characterization of the individual components and their interactions. For self-propelled particles, intrinsic complexity stems from the fact that the polar nature of the colloids necessitates that the interactions depend on positions and orientations of the particles, leading to a $2d-1$ dimensional configuration space for each particle, in d dimensions. Moreover, the interactions between such non-equilibrium colloids are generically non-reciprocal, which makes the characterization even more complex. Therefore, derivation of generic rules that enable us to predict the outcomes of individual encounters as well as the ensuing collective behavior will be an important step forward. While significant advances have been made on the theoretical front, such systematic experimental characterizations using simple artificial systems with measurable parameters are scarce. Here, two different contrasting types of colloidal microswimmers are studied, which move in opposite directions and show distinctly different interactions. To facilitate the extraction of parameters, an experimental platform is introduced in which these parameters are confined on a 1D track. Furthermore, a theoretical model for interparticle interactions near a substrate is developed, including both phoretic and hydrodynamic effects, which reproduces their behavior. For subsequent validation, the degrees of freedom are increased to 2D motion and resulting trajectories are predicted, finding remarkable agreement. These results may prove useful in characterizing the overall alignment behavior of interacting self-propelling active swimmer and may find direct applications in guiding the design of active-matter systems involving phoretic and hydrodynamic interactions.

1. Introduction

The non-equilibrium dynamics and self-organization of active matter is a fascinating topic with recent intense developments, constituting a wide range of systems that span across many scales, from single molecules to colonies of cells and whole organisms.[1] Importantly, studies of active matter systems lend themselves to systematic coarse-graining approaches that can connect microscopic features of every particular system to the scale in which the collective emergent properties of the system are studied, in the spirit of "more is different".[2] Key to this program is characterization of the microscopic interactions between the individual agents in the system. A well-studied model system for a self-propelled particle constitutes a spherical Janus colloid with asymmetric catalytic activity[3] that has been realized using Pt-catalyzed H_2O_2 degradation,[4,5] and then extended to many different systems relying on a variety of chemical reactions[6,7] and physical effects.[8] More recently, active colloids have been placed in increasingly complex environments, often with the intention of creating smart material structures that can be controlled via the active components. The complexity is increased using either passive particles,[9,10] introducing environments that are characterized by viscosity,[11] or chemical equilibria,[12] and by introducing new capabilities like information processing.[13,14] A plethora of different types of collective dynamics in such phoretic active colloids has been theoretically

P. Sharan, J. Simmchen
Chair of Physical Chemistry
TU Dresden
01062 Dresden, Germany
E-mail: JULIANESIMMCHEN@GMX.NET

The ORCID identification number(s) for the author(s) of this article can be found under https://doi.org/10.1002/smll.202300817

DOI: 10.1002/smll.202300817

A. Daddi-Moussa-Ider, J. Agudo-Canalejo, R. Golestanian
Max Planck Institute for Dynamics and Self-Organization (MPIDS)
37077 Göttingen, Germany
E-mail: ramin.golestanian@ds.mpg.de

R. Golestanian
Rudolf Peierls Centre for Theoretical Physics
University of Oxford
Oxford OX1 3PU, UK

J. Simmchen
Pure and applied chemistry
University of Strathclyde
G11XL Glasgow

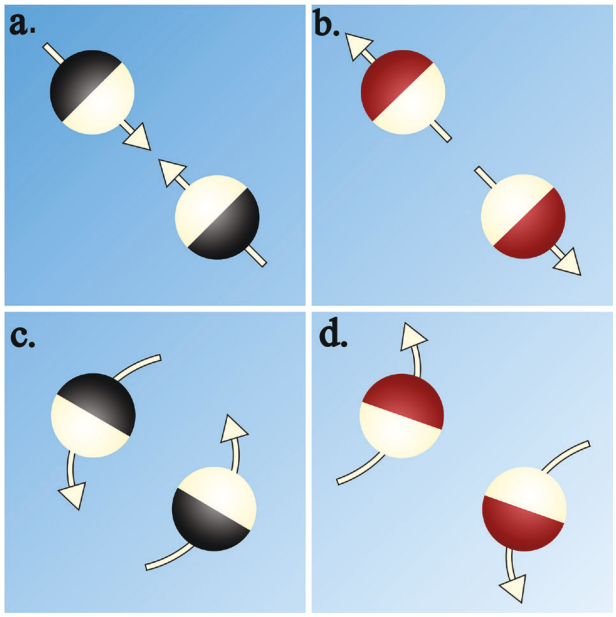

Figure 1. Exemplary dynamical states for two interacting chemically active colloids. A pair of active colloids shows various types of mutual interactions depending on their phoretic mobilities, chemical activities, and geometrical configuration. In an axisymmetric configuration, the two particles can move either a) toward or b) away from each other. Non-reciprocal types of interaction occur during which the particle are either c) attractively or d) repulsively scattered from each other. Here and in what follows, black caps (a,c) and red caps (b,d) represent Pt@SiO_2 and Cu@SiO_2 Janus colloids, respectively.

predicted[15–21] and experimentally observed.[22–26] Here, we set out to characterize the pair interaction of such catalytically active colloids and thereby provide the key ingredient for prediction and engineering of complex collective properties of ensembles of such self-propelled particles. While our specific focus is on synthetic active matter systems, we note that similar studies have been performed in a variety of biological systems ranging across scales, from bacteria [27] to large scale organisms such as fish[28] and birds.[29,30]

Interactions among individuals, and in particular, two-body interactions have been a topic of interest from a theoretical perspective. For self-phoretic colloids [31,32] driven by interfacial transport processes (phoresis), a number of theoretical studies have considered in detail the possible dynamics arising from colloid-colloid interactions.[33–37] In general, such pairwise interactions are mediated by the intervening solution between the two colloids. More specifically, the total interaction comprises contributions from the hydrodynamic flows and the phoretic fields, that is, gradients in the concentrations of solutes or the corresponding chemical potential, in response to which the colloids experience phoretic drift. **Figure 1** shows a few typical states assumed by two interacting chemically active colloids. Various classes of interactions occur depending on the chemical activity, phoretic mobility, and geometrical arrangement of the pair of active colloids.[35] These include mutual approach or escape along the line connecting the centers of the spheres (Figure 1a,b), in addition to more complex non-reciprocal interactions consisting of attractive or repulsive scattering (Figure 1c,d), when considering motion in two dimensions. When both hydrodynamic and phoretic interactions are accounted for, a pair of two active Janus particles can assemble or escape from each other depending on their catalytic/active coverage and orientation of approach.[33] Notably, if these interactions are attractive, geometrically anisotropic clusters can emerge from isotropic colloids, that can induce motility which would otherwise not be feasible in isotropic systems.[34,38] Along these lines, Nasouri et al. showed that when the two colloids are sufficiently close (with the gap size smaller than particle diameter), neighbor-colloid induced motion and self-generated neighbor-reflected motion dominate, resulting in behaviors which cannot be fully explained by the often-used far-field approximation.[36,37] These results highlight the relevance of near-field dynamics. However, it is also important to note that all these previous studies focused on interparticle interactions in unconfined space, without taking into account the presence of a nearby wall, which is the usual experimental situation, as colloids typically sediment to the bottom of the experimental chamber.

Despite the abundant theoretical research on pair interactions just described, they have very rarely been studied in detail in experimental systems. Wykes et al. and Jewell et al. presented pairwise and collective assembly of tripartite metallic rods via hydrodynamic and electrophoretic interactions in two separate studies.[39,40] When the isotropic metallic rods are designed to induce extensile type (pusher) surface flows, these rods self-assemble into a rotor or a swimmer in agreement with theoretical predictions.[41] In contrast, when the flow is reversed to a contractile (puller) flow, such assemblies are temporary and disassemble on a much shorter time scale than the pusher-type counterpart. Interestingly, these studies also point to the relevance of distinctive flow fields[42] that might induce contrasting pair interactions. Similar to bimetallic rods, Baker et al. reported formation of dimers in 3D printed Janus tori structures.[43] A very recent work of Katuri et al. examines electrically driven platelets, a novel form of the simplest interacting system which completely avoids chemical interactions and creates activity purely based on electric interactions.[44]

Our aim is to build on the existing purely theoretical studies or empirical observations that have been performed for studying two-body interactions, and capture the full breadth of the available parameter space. In laboratory settings, typically, studying such pairwise interactions is not straightforward because of the interfering many-body interactions. Additionally, pair interactions of active particles with contrasting flow fields should be compared for a more thorough understanding of such complex dynamics. Therefore, here we study in detail how two different types of Janus particles,[45–48] each with distinctive surface flows, interact with each other near a rigid substrate. We explore in detail simple two-body interactions in one dimension. The experiments are accompanied by a detailed theoretical analysis of pair interactions in the presence of the bottom substrate wall of the chamber. This allows us to extract all the relevant parameters of active colloids (activities and mobilities), which we then use for an accurate reproduction of our experiments in two dimensions using numerical simulations. We therefore expect our experimental technique and the accompanying theory to become the foundation for future work not only on collective interactions among active particles, but also between mixtures and systems showing non-reciprocal interactions. These

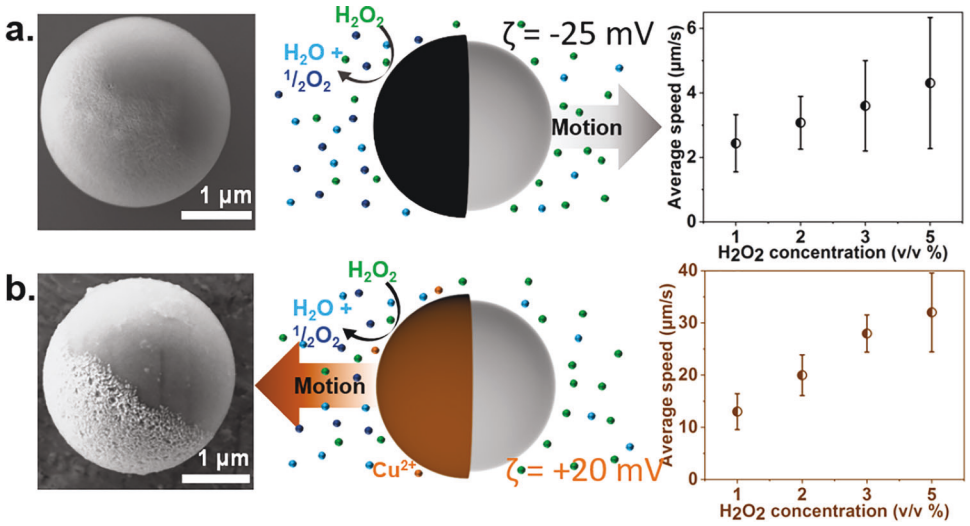

Figure 2. Two types of active Janus colloids studied in the present work. Scanning electron microscopy (SEM) image, scheme representing illustrative propulsion mechanism and average speed of a) $Pt@SiO_2$ and b) $Cu@SiO_2$ Janus micromotor in varying H_2O_2 concentrations. H_2O_2 decomposition involves several intermediate steps, but for simplicity the schematics indicate a one step decomposition into oxygen and water.[4]

outcomes will be pivotal for designing innovative materials based on anisotropic interactions and applications taking benefit from such phenomena.[49,50]

2. Results

2.1. $Pt@SiO_2$ and $Cu@SiO_2$ Active Colloids

We begin by introducing the two different types of spherical Janus active colloids which have been used in this work. The first one is the well studied $Pt@SiO_2$ micromotor, which propels itself forward by catalyzing the decomposition of H_2O_2 on the Pt half.[4,51] These self-generated chemical gradients create a flow in the close vicinity of the particle (phoretic slip) which propels the particles in the direction away from the catalytic cap (inert-forward). Potentially, due to different thicknesses of the catalyst, different reaction rates are assumed to create an additional electric field, leading to the observed magnitude of motion.[52,53] An alternative explanation could be the occurrence of ionic intermediates, leading to ionic diffusiophoresis.[54] Depending on whether the averaged surface slip is strongest on the 'leading face' or on the 'trailing face' of the microswimmer, the motion direction is determined.[55,56] It is challenging to account for slips due to all the propulsion mechanisms (diffusiophoretic, electrophoretic, etc.), calculate the slip exactly, and determine the precise flow fields to resolve the pusher/puller character. In this context, Campbell et al. experimentally evaluated the flow field around similar, but larger particles, finding that they resemble that of a pusher, whereby the swimmer pushes the fluid along the propulsion axis and draws fluid from the sides (**Figure 2**a).[42] Notably, the $Pt@SiO_2$ colloids show enhancement in motion as the hydrogen peroxide concentration is increased, with a typical speed of about 4 μm s^{-1} at 5% H_2O_2 concentration (Figure 2a and Video S1, Supporting Information).

The second swimmer type is a Janus $Cu@SiO_2$ active colloid. Likewise, it can achieve self-propulsion by catalyzing the decomposition of H_2O_2 on the metal hemisphere (see Figure 2b and Video S2, Supporting Information).[45,46] The major noticeable difference with respect to the $Pt@SiO_2$ micromotors is the release of a small but not insignificant quantity of Cu^{2+} ions, inverting the overall charge of the colloid to a positive value and the propulsion direction. The self-propulsion mechanism is therefore likely to be dominated by ionic diffusiophoresis with a certain self-electrophoretic influence, similar to silver-based motors.[57] A self-electrophoretic model based on pole to equator surface flow, owing to a positive zeta potential on the Cu cap and a negative value on the SiO_2 half leading to a stronger surface gradient of potential on the Cu side, resulted in good agreement with experimentally observed behaviors in externally applied flow.[45] The overall result is that the orientation and swimming mode of these colloids resemble their galvano-phoretic cousins [6] swimming cap-forward. Similarly to the $Pt@SiO_2$ colloids, the $Cu@SiO_2$ motors also demonstrate an enhancement in motion with increasing hydrogen peroxide, resulting in higher speeds and an enhanced directionality. However, due to different charge conditions, stemming most likely from the release of some copper ions, the system is more complex.

2.2. 1D Experimental Dynamics

To carefully differentiate and characterize the pair interaction between two active colloids, we restrict their degrees of freedom to one dimension and study the resulting interactions correspondingly. Briefly, to restrain their motion in the *x* direction and facilitate head-to-head interaction of two particles (when the propulsion axis of the two active particles is pointing toward each other, see Supporting Information), we performed these experiments on confined tracks. Experimentally, we used cracks carved on a SU8 photoresist coated glass substrate (**Figure 3**a) where the colloids are forced to follow these restricted paths (only occasionally we observed these colloids to manoeuvre out of the crack).

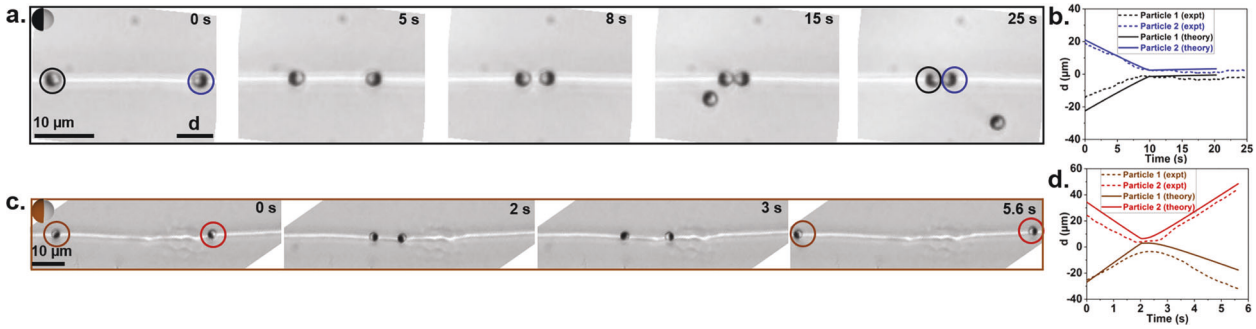

Figure 3. Pair interaction in a confined geometry (1D interaction). a) Time lapse optical images of interaction between two Pt@SiO_2 particles on a confined track indicated by white lines. b) Experimentally and theoretically calculated trajectories of the two Pt@SiO_2 particles with respect to time, in confinement. The two particles reach a stable steady state configuration after physical contact. c) Time lapse optical images of pair interaction between two Cu@SiO_2 particles on a confined track. d) Experimentally and theoretically calculated trajectories of the two Cu@SiO_2 particles with respect to time, in confinement. After getting in close vicinity, the two particles reorient themselves and move apart from each other.

When placed on such cracks, both active colloids (Pt@SiO_2 and Cu@SiO_2) behave very similarly to when they are in a non-confined environment, that is, they propel with their propulsion axis parallel to the Janus normal, and their out-of-plane rotation (θ, **Figure 4**b inset) is restricted by activity.[51].

When two Pt@SiO_2 active colloids happen to be placed in one crack moving toward each other, they seem to not take notice of each other, until coming into very close contact. We define this term when the distance between the centers of two interacting particles is about one particle diameter or 2*a*, where *a* is the radius of a particle. After contact, they seem to interact sterically and push each other, without undergoing significant displacement (Figure 3a and Video S3, Supporting Information). The observed behavior is well reproduced by the theoretical model, which finds that two Pt@SiO_2 active colloids moving in 1D will reach a steady sate in which the propulsion forces are balanced by the steric forces, as will be explained in detail below (Figure 3b).

In contrast, when two Cu@SiO_2 particles head toward each other in confinement, they seem to detect each other's presence at larger distances (> 7*a*). Instead of pushing against each other, while still at a large separation distance both particles independently reorient and head back, away from one another along the same path (Figure 3c and Video S4, Supporting Information). Quite noticeably, these particles demonstrate mutual repulsive interactions, which depend on activity. Different degrees of activity can be reached by modulating the fuel content of the environment and differently to the Pt@SiO_2 motors, the interaction for Cu@SiO_2 colloids show activity dependence: the distance at which the particles take notice of each other increases with the fuel concentration (Figure S30, Supporting Information) and Videos S10 and S11 (Supporting Information). An analogous alignment behavior can be recovered by our analytical model described below, where the direction of motion of two Cu@SiO_2 is found to be reversed after the pair comes into close vicinity (Figure 3d).

Let us now look in depth at both cases separately. For this purpose, we define the particle's orientation and the corresponding in-plane or azimuthal angle (ϕ) and out-of-plane or zenith angle (θ) in the inset of Figure 4b (Supporting Information). In the case of Pt@SiO_2 colloids, the in-plane angle (ϕ) is nearly constant (within experimental errors) even after their close contact, as is also noted in the time lapse optical images in Figures 3a (Figure 4a). In addition, the zenith angle remained nearly unchanged with slight deviations in the experimental measurements most likely stemming from crack irregularities or can be attributed to the effect of thermal noise (Figure 4b). Additionally, we plot the

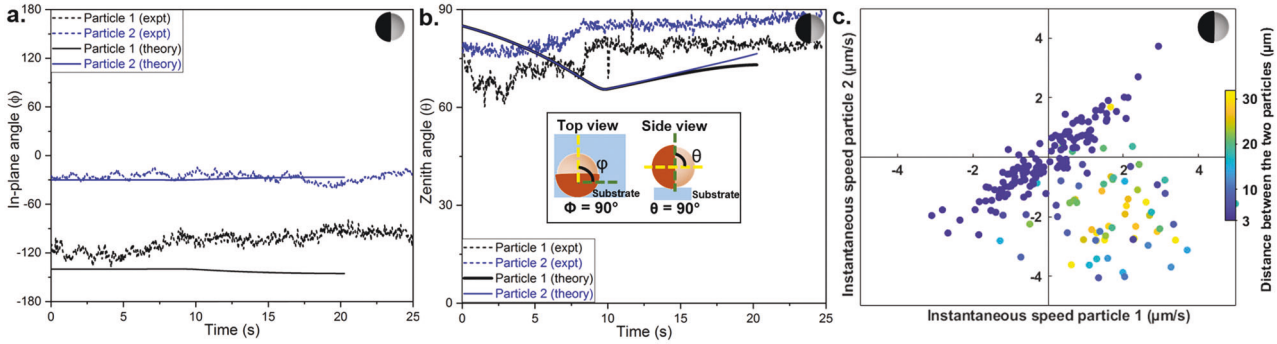

Figure 4. Steric interaction between two Pt@SiO_2 active colloids. Experimental and theoretical data indicating change in a) in-plane angle and in b) zenith angle or polar angle with respect to time, for the two Pt@SiO_2 colloids reported in Figure 3a. Nearly no change in these parameters even after the two Pt@SiO_2 colloids get in contact with each other indicate no-repulsive interaction. c) Correlation between instantaneous speed of the two Pt@SiO_2 colloids reported in Figure 3a, with respect to the interaction distance between them. Positive speed indicates motion in the right direction and negative speed indicates motion in the left direction. The instantaneous speed has been plotted every 5 frames.

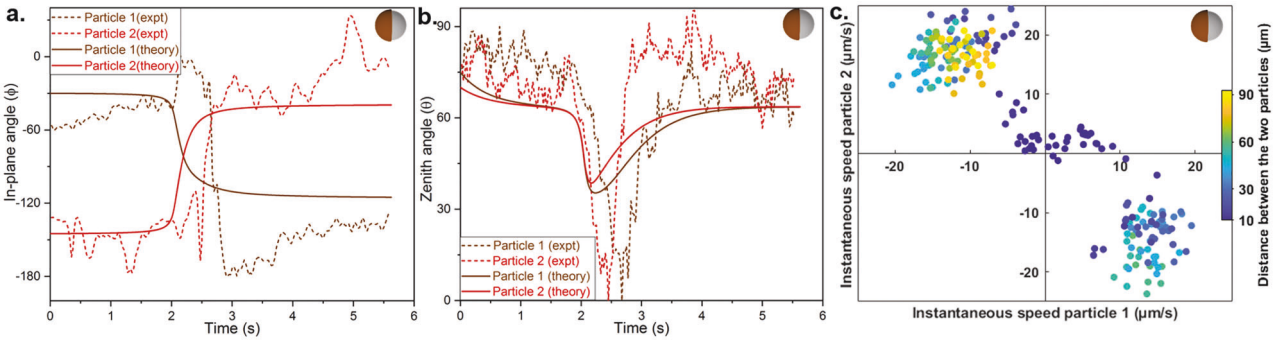

Figure 5. Repulsive interaction between two Cu@SiO_2 active colloids. Experimental and theoretical data indicating change in a) in-plane angle and in b) zenith angle or polar angle with respect to time, for the two Cu@SiO_2 colloids reported in Figure 3c. Prominent changes in these parameters after the two Cu@SiO_2 colloids get in close vicinity of each other indicate repulsive interaction between them. c) Correlation between instantaneous speed of the two Cu@SiO_2 colloids reported in Figure 3c, with respect to the interaction distance between them. Positive speed indicates motion in the right direction and negative speed indicates motion in the left direction. The instantaneous speed has been plotted for every frame.

correlation between the instantaneous speeds of the two particles with respect to the distance between each other, where positive and negative speeds indicate particles moving toward the right and left, respectively (Figure 4c and Supporting Information). Initially, the particles approach each other, with opposite-sign velocities $v_1 > 0$ and $v_2 < 0$, located in the lower-right quadrant. After their encounter, when steric interactions set on between the two Pt@SiO_2 colloids, they form a pair and move together, resulting in data points within the bottom-left and top-right quadrants that are concentrated along the line of perfect correlation $v_2 = v_1$.

In the case of Cu@SiO_2 colloids, we record a nearly constant in-plane angle (ϕ) and out-of-plane angle (θ) (within experimental errors) until the particles reach the vicinity of each other (**Figure 5**a). Once the repulsive interaction sets in, we notice a stark change in the angle (ϕ), which correlates to the reversal of the swimming direction as indicated in the time lapse optical images in Figure 3c. This reversal in swimming direction is facilitated by an out-of-plane rotation of the particle and, accordingly, we notice the zenith angle drop instantaneously from around 90° to 0°, to allow flipping of particles (Figure 5b). Once the change in swimming direction has been achieved, the particles regain their original swimming orientation which is close to $\theta = 90°$. A minor discrepancy between the theory and the experiment can be seen in the behavior of Cu@SiO_2 particles in Figure 3d: in the experiment, the particles turn around before contact, whereas in the theory the particles first come into contact and soon after turn around. This small discrepancy may be attributed to additional effects not included in the theory, in particular the lack of near-field hydrodynamics, which are typically repulsive and prevent direct contact between colloids; the roughness (topographical structure) of the channel; or potential additional effects of ionic origin not accounted for in our description of diffusiophoresis. Accounting for these additional effects in the present context is rather complex and would only lead to minor improvements in the description. Moreover, thermal effects play a non-negligible role in the observed scattering events, because the swimming trajectories become fluctuating. In summary, we doubt that improving the deterministic model by accounting for the above-mentioned additional effects would necessarily lead to a significantly better match with the experimental observations.

In addition, it is worth noting that the reorientation of active colloids is not caused by rotational diffusion, but rather by the diffusiophoretic-hydrodynamic interactions. The rotational diffusion time can be calculated in a bulk fluid to be around $D_r^{-1} = 8\pi\eta a^3/(k_B T) \approx 25$s using the experimental parameters. This time is expected to be even larger near a confining wall since diffusion is hindered. Accordingly, the rotational diffusion time is much larger than the reorientation time of Cu@SiO_2 which is found to be around 2s; see Figure 5a. Finally, we mention that accounting for thermal noise in our theoretical description still yields good matching with the experimental results. Since our goal in the 1D experiments was to estimate the mobility and activity parameters, we preferred to base our comparison on the deterministic trajectories and look for the combination of parameters that lead to the best fit with the experimentally observed trajectories.

In the correlation graphs for the instantaneous speeds of these two particles (Figure 5c), the data points are initially located in the bottom-right quadrant ($v_1 > 0$ and $v_2 < 0$), while the particles head toward each other. Then, we observe a non-reciprocal turning event where particle 1 quickly turns around (v_1 changes from positive to negative) while particle 2 is almost static ($v_2 \approx 0$). Finally, particle 2 turns around as well and data points locate to the top-left quadrant ($v_1 < 0$ and $v_2 > 0$), as the particles move away from each other.

2.3. 2D Experimental Dynamics

In the experimental system, once we remove the confinement, the interactions are extended to the 2D space, and the particles are free to move in the *xy* plane. We recorded a similar interaction behavior of the particles without any confinement: the Pt@SiO_2 colloids execute steric interactions and the Cu@SiO_2 particles demonstrate repulsive interactions. For better understanding, we grouped these 2D interactions into three categories: <90°, 90° and >90° (**Figure 6**). When the two particles encounter with their propulsion axis toward each other, it is labeled <90° incident, and so on. Irrespective of their encounter angles, the two Pt@SiO_2 colloids do not seem to notice each other and eventually collide. Upon contact, they no longer continue to push against each other,

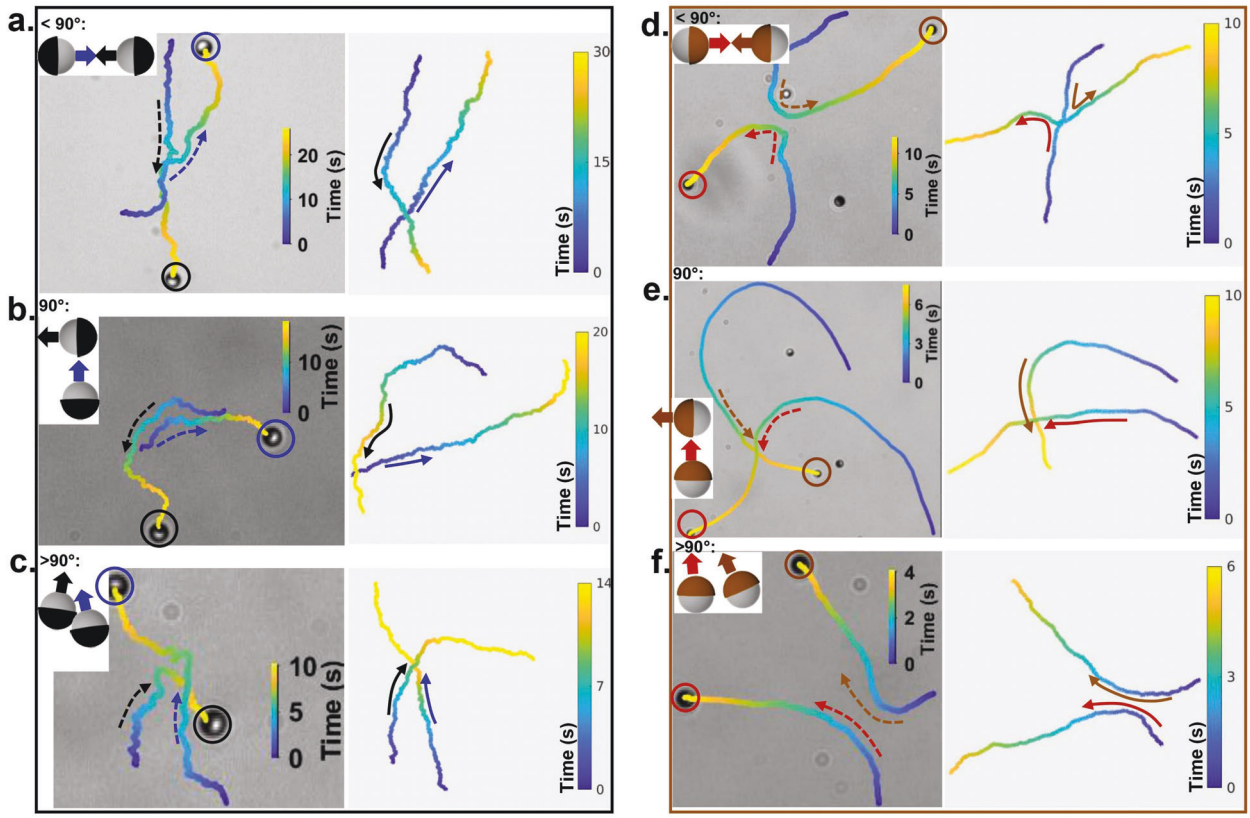

Figure 6. Pair interaction without confinement (2D interaction). Experimental trajectories (optical images) and the corresponding theoretically calculated trajectories (both with trajectories color coded according to time) illustrating pair interaction between a,b,c) two Pt@SiO_2 and d,e,f) two Cu@SiO_2 colloids at various angles (<90°, 90°, and >90°).

rather they slide adjacent to one another over a time scale of 3 – 4 s and finally escape. This escape is now facilitated by the absence of confinement and hence free in-plane rotation, which was absent in the case of 1D interactions in the crack. No significant change in the particle speeds is noted throughout their interaction incident (see Video S5, Supporting Information).

In contrast, the Cu@SiO_2 particles seem to take notice of one another even from a distance (>7a), regardless of their encounter angles (Figure 6d,e,f and Video S6, Supporting Information). Their encounter results in a scattering event, whereby, upon entering each others interaction range, the two particles (or sometimes only one) almost stall for a few seconds in order to reorient in-plane and change their motion direction away from each other. The encounter is marked by a sharp reduction in the particle speed, which is regained after the scattering event.

2.4. Theoretical Hydrodynamic Model

In our theoretical model, we consider a pair of Janus particles moving in a quiescent viscous fluid in the limit of low Reynolds and Péclet numbers. Under these conditions, the fluid dynamics is governed by the steady Stokes equations $-\nabla p + \eta\nabla^2 v = 0$ and $\nabla \cdot v = 0$ with v and p denoting the fluid velocity and pressure fields, respectively. In addition, the concentration field $c(r)$ of the solute molecules satisfies the Laplace equation $\nabla^2 c = 0$. Accordingly, the hydrodynamic and phoretic problems can conveniently be decoupled from each other in this approach.

At the surface of the active colloids, the radial flux of the solutes is related to the chemical activity α via the boundary condition $-D\hat{n} \cdot \nabla c = \alpha(\hat{n})$ at $r = a$, with D denoting the diffusion coefficient of the solute molecules, $\hat{n}$ the unit vector normal to the particle surface pointing outward, and a the particle radius. For a Janus active colloid, we set $\alpha = 1$ on the chemically active hemisphere and $\alpha = 0$ on the inert part. We assume that the active colloids are set to motion through a slip velocity, v_S, resulting from a gradient of concentration that is locally induced via a surface chemical reaction. Accordingly, $v_S = \mu\nabla_{\|} c$ holds at the surface of the active colloids, with μ denoting the phoretic mobility and $\nabla_{\|}$ the tangential gradient operator. Both the chemical activity and phoretic mobility functions are expanded into Legendre polynomials following the usual approach. In addition, the nonpermeability boundary condition at the surface of the substrate implies a vanishing normal flux such that $\partial_z c = 0$ at the plane $z = 0$. We denote by c_∞ the concentration far away from the surfaces of the swimmers and the interface.

For the determination of the translational and rotational velocities of the active colloids in the presence of a confining wall, we employ the well-established image solution technique to describe the hydrodynamic and phoretic fields in the far field (Methods). In addition, we introduce steric (excluded-volume) interactions as the particles get closer, so as to avoid unphysical overlap. The

two particles of equal radius a are a distance ℓ apart from each other and are located at height h above the substrate. We define the dimensionless numbers $\epsilon = a/h$ and $\delta = a/\ell$ and focus on the limit of far-field interactions such that $a \ll h$ and $h^2 \ll a\ell$ so that $\delta \ll \epsilon^2$. We note that the far-field approximation is a well-established approach and has widely been used in the context of hydrodynamic interactions in confinement.[58–63]

As shown in Methods, the present problem can be decomposed into three sub problems: (i) intrinsic self-propulsion without background phoretic or hydrodynamic fields, (ii) phoretic drift due to an external concentration field, that is, the phoretic motion of particle 2 due to the gradient in the chemical field induced by particle 1, and (iii) hydrodynamic drift due to an external flow field, that is, the swimming dynamics of particle 2 due to the hydrodynamic field induced by particle 1.

The resulting induced swimming speed and rotation rates can then be expressed using a perturbative approach in terms of power series of the dimensionless parameters ϵ and δ. Both the diffusiophoretic (D) and hydrodynamic (H) contributions to the swimming velocities can be decomposed into self (S) and pair (P) induced interactions. Then, The dynamical equations governing the motion of the two active colloids can be written by combining the self and pair interactions as

$$\frac{\mathrm{d}x_i}{dt} = V_i^{\mathrm{S}} + V_i^{\mathrm{P}}\,, \tag{1a}$$

$$\frac{\mathrm{d}\hat{u}_i}{\mathrm{d}t} = \left(\boldsymbol{\Omega}_i^{\mathrm{S}} + \boldsymbol{\Omega}_i^{\mathrm{P}}\right) \times \hat{u}_i\,, \tag{1b}$$

for $i \in \{1, 2\}$, with i is the index of each particle. Here, $\hat{u}_i$ denotes the orientation of the ith particle in the lab frame.

2.5. Modeling 1D Interactions

We now consider a pair of active colloids restricted to move along a crack; see Figure S4 (Supporting Information) for a graphical illustration of the system setup. The orientations of the two colloids are determined by the angles $(\phi)_i$ and θ_i as defined in Figure 4b. We examine for simplicity the deterministic case in the absence of thermal noise and consider a perfectly symmetric configuration in which $\theta_2 = \theta_1$ and $(\phi)_1 = (\phi)_2 + \pi$. We further introduce the notation $\theta \equiv \theta_1 = \theta_2$ and $(\phi) \equiv (\phi)_1$. In addition, we assume that the two particles are initially located at positions $x_2 = (-\ell/2, 0, h)$ and $x_1 = (\ell/2, 0, h)$. It is worth mentioning that the following theoretical developments are performed for a symmetrical configuration so as to obtain approximate expressions of the translational and rotational velocities. This will allow us to identify the key parameters governing the overall alignment behavior of the pair of active colloids. However, the theoretical predictions shown in Figures 3, 4, and 5 have necessarily been performed by considering an asymmetric configuration, allowing for a better match with the experimental results.

We now expand both the activity and mobility functions in terms of Legendre polynomials as $\alpha(\hat{n}) = \sum_{k\geq 0} \alpha^{(k)} P_k(\hat{u}\cdot\hat{n})$ and $\mu(\hat{n}) = \sum_{k\geq 0} \mu^{(k)} P_k(\hat{u}\cdot\hat{n})$, respectively. We further define for $k \in \{1, 2\}$ the dimensionless parameters $A^{(k+1)} = \alpha^{(k+1)}/\alpha^{(0)}$ and $M^{(k)} = a\alpha^{(0)}\mu^{(k)}/D^2$, which can be viewed as scaled activity moment and mobility moment, respectively. The time variation of the interparticle distance is obtained (see Experimental Section) as

$$\frac{a\dot{\ell}}{D} = -2\left(\mathrm{Pe}\sin\theta + q\epsilon^2\sin 2\theta\right)\cos\phi + 4M^{(0)}\,\delta^2\,, \tag{2}$$

with $\mathrm{Pe} = -(1/15)(5A^{(1)}M^{(0)} + 2A^{(2)}M^{(1)})$ the Péclet number based on the swimming speed of the active colloid in a bulk fluid, which describes the ratio between advection and diffusion time scales. In addition, $q = (3/32)(2A^{(2)}M^{(0)} + A^{(1)}M^{(1)})$. In turn, the scaled temporal evolution of the polar and azimuthal angles is governed by

$$\frac{a^2\dot{\theta}}{D} = -\left[f\left(\epsilon^2 + 8\delta^3\epsilon^{-1}\right) - \left(q+g\right)\epsilon^3\cos\theta\right]\sin\theta - 8\delta^2\left(f + 4q\delta\sin\theta\cos\phi\right)\cos\theta\cos\phi\,, \tag{3a}$$

$$\frac{a^2\dot{\phi}}{D} = 8\delta^2\left(f\,\csc\theta + 4q\,\delta\cos^2\theta\cos\phi\right)\sin\phi\,, \tag{3b}$$

where we have defined the abbreviations $f = 3M^{(1)}/16$ and $g = 3A^{(1)}M^{(1)}/64$. In the far-field limit, it can be shown that the dynamical system of equations admits a fixed point at $\theta = \theta_0$, where $\theta_0 \equiv \arccos(f/[\epsilon(q+g)])$, and $(\phi) = 0$.

In the case of platinum-half-coated active colloids, the experiments show that both the polar and azimuthal angles remain typically constant. Assuming that the Janus motors are initially aligned parallel to the interface such that $\theta \sim \pi/2$, it can readily be shown that $h^2\dot{\theta}/D \sim -(3/16)\,M^{(1)}(1 + 8(h/\ell)^3)$ and $d^2\dot{\phi}/D \sim (3/2)\,M^{(1)}\phi$. Thus, it is expected in this case that $M^{(1)} \ll 1$ so that both the polar and azimuthal orientations do not vary significantly during the mutual approach of the two particles. As will be shown below, $M^{(1)} > 0$, so that the azimuthal angle features a downward trend before increasing at short interparticle distances; see the theoretical curve in Figure 4b. Ultimately, the pair reaches a steady state configuration in which the propulsion forces are balanced by the steric forces.

On the other hand, the situation of copper-half-coated active colloids shows a fundamentally different reorientation mechanism during which the azimuthal orientation is abruptly increased as the two particles come into close vicinity. This behavior is accompanied by a sharp decrease in the polar angle, which after reaching the minimum, relaxes back to a steady value. Upon particle contact, the direction of motion is reversed and the two particles move away from each other while maintaining a quasi-parallel orientation with respect to the wall. Correspondingly, it is expected that the value of $M^{(1)}$ would for $Cu@SiO_2$ be significantly larger than that for $Pt@SiO_2$.

To explain the observed alignment behavior, we express the key parameter $M^{(1)}$ governing the reorientation dynamics of the pair in terms of the chemophysical properties of the active colloids. For that aim, we assume that the phoretic mobility scales linearly with the zeta potential of the active particles.[5,58,64] Denoting by μ_+ and μ_- the phoretic mobility of the front and back caps, respectively, it follows that the zeroth and first moments of the phoretic mobility are given as $\mu^{(0)} = (1/2)(\mu_+ + \mu_-)$ and $\mu^{(1)} = (3/4)(\mu_+ - \mu_-)$, respectively. By noting that $\mu^{(0)}M^{(1)} = \mu^{(1)}M^{(0)}$, it follows then that $M^{(0)} = 4M^{(1)}/(3Q)$, wherein $Q = \Delta\zeta/\bar{\zeta}$ with $\Delta\zeta = \zeta_+ - \zeta_-$ and $\bar{\zeta} = (1/2)(\zeta_+ + \zeta_-)$. For $Pt@SiO_2$ active colloids, we

expect a value of $\zeta_- \equiv \zeta_{Pt} = -25$ mV and $\zeta_+ \equiv \zeta_{SiO_2} = -30$ mV, leading to $Q = +0.2$. For Cu@SiO_2 active colloids, $\zeta_- \equiv \zeta_{SiO_2} = -30$ mV and $\zeta_+ \equiv \zeta_{Cu} = +20$ mV, which yields $Q = -10$. Then, it follows upon substitution of $M^{(0)}$ into the expression for Pe that $M^{(1)} = -(45/2)\,\mathrm{Pe} \Big/ (10A^{(1)}/Q + 3A^{(2)})$. As shown below, from fits to the experimental data we find for both types of active colloids that $A^{(1)}/Q$ and $A^{(2)}$ are negative numbers so that $M^{(1)} > 0$. Accordingly, $M^{(1)}$ scales linearly with Péclet number, so that the larger the Péclet number the more likely the pair will reorient and move away from each other after physical contact.

In our approach, the only fitting parameters to be extracted from the experiments are the scaled activity moments $A^{(1)}$ and $A^{(2)}$ because the zeroth and first scaled moments of the phoretic mobility can both be expressed in terms of $A^{(1)}$ and $A^{(2)}$. It would indeed be ideal to estimate parameters with error bars. However, we believe that averaging over multiple trajectories is far from being within reach because timings are highly irregular and the averaging over multiple cases is not really viable due to very different timings. Owing to the highly fluctuating nature of the swimming trajectories and the fact that the observed scattering events feature quantitatively different behaviors in each experimental realization, we qualitatively estimate the values of $A^{(1)}$ and $A^{(2)}$ providing the best visual match between theory and experiments.

By considering typical swimming velocities $V = 3\tilde{}\mu\mathrm{m\ s^{-1}}$ for Pt@SiO_2 and $V = 16\tilde{}\mu\mathrm{m\ s^{-1}}$ for Cu@SiO_2, it follows that the Péclet numbers $\mathrm{Pe} = aV/D$ for platinum- and copper-half-coated colloids are $\mathrm{Pe}_{Pt@SiO_2} \simeq 0.002$ and $\mathrm{Pe}_{Cu@SiO_2} \simeq 0.012$, respectively. Here, we have used $a = 1.5\tilde{}\mu\mathrm{m}$ and $D = 2 \times 10^{-9}\ \mathrm{m^2\ s^{-1}}$. For Pt@$SiO_2$, the best fit of the experimental data, displayed as the solid lines in Figure 4a,b, is given by $(M^{(0)}, M^{(1)}) = (0.0006, 0.0001)$ and $(A^{(1)}, A^{(2)}) = (-10, -1)$. For Cu@$SiO_2$, see Figure 5a,b, we obtain $(M^{(0)}, M^{(1)}) = (-0.0012, 0.0093)$ and $(A^{(1)}, A^{(2)}) = (2, -9)$. Using these parameter values, we find that $\theta_0 \approx 95°$ for Pt@SiO_2 and $\theta_0 \approx 63°$ for Cu@SiO_2 where we assumed that $h = 1.2a$. In both cases, the model recovers correctly not only the behavior of both angles for each particle, but also the behavior of the interparticle distance over time, see Figure 3b,d.

It is worth noting that the correlation between Péeclet number and reorientation its not due to advective effects that induce reorientation. The correlation comes from the fact that the phoretic mobility asymmetry on the surface of the colloid (governed by the phoretic mobilities μ_+ and μ_- of each cap) affects both the self-propulsion velocity (which determines Pe) and the reorientation of the particle. By quantifying these relations, we have shown that one can express the reorientation strength as being proportional to Pe. This is not a "causal" relation between the two, but rather only a reflection of the fact that both Pe and the reorientation strength have the same origin, in particular both are proportional to $M^{(1)}$ (which quantifies the phoretic mobility surface pattern). A similar relation between Pe and the reorientation strength has been discussed in Ref. [65].

2.6. Modeling 2D Interactions

With the parameter values obtained from the theoretical fits to 1D interparticle interactions in hand, we can apply our theory to unconfined interactions in the 2D plane. Without any additional fit parameters, we are able to reproduce the key features of 2D interactions, including <90°, 90°, and >90° collisions, for both Pt@SiO_2 and Cu@SiO_2 colloid pairs. The theoretical trajectories are displayed side-by-side with the corresponding experimental trajectories in Figure 6, showing remarkable agreement.

Importantly, this agreement serves as proof of concept that chemo-hydrodynamic parameters extracted from control experiments in our 1D set up can later be used for computational modeling of more complex behaviors. In particular, future work may explore the use these parameters together with the equations of motion derived in this work for the microscopic understanding of the origin of motion reversal, as well as the prediction of collective behavior in denser collections of active colloids, including, for instance, mixtures of Pt@SiO_2 and Cu@SiO_2 colloids. While, as described above, the use of a far field approximation prevents us from fully capturing the finer details of the interaction when the particles come very close to each other (Figure 3d), far field interactions are sufficient to describe the large-scale instabilities that arise in an initially dilute suspension,[17] and repulsive near field hydrodynamics often only act to prevent contact between the particles, and thus set a larger effective radius for them.

3. Discussion

We have introduced here an experimental setup that allows for the study of pair interactions between active particles, in a controlled environment (see **Table 1**). Thanks to the 1D confinement, which reduces rotational diffusion and forces the particles to encounter each other, a characterization of the detailed time-dependence of the particle–particle distance as well as particle orientations becomes possible. This further allows for fitting to a theoretical model, and ultimately to the extraction of the key material parameters that define the particles, which in our system of catalytic Janus swimmer include the catalytic activity and phoretic mobility patterns at the surface of the particles.

To this end, we also developed a theory for the pair interactions between catalytic Janus swimmers near a wall (corresponding to the bottom substrate of the chamber), including both phoretic interactions mediated by the concentration fields of the chemicals involved in the reaction, as well as hydrodynamic interactions mediated by the flow fields induced by the swimmers. While both the behavior of a single particle near a wall [66] and pair interactions in unconfined space [17] had been studied before, a theory for interparticle interactions near a wall was still lacking. Given that, in most experiments with active colloids, these sediment to the bottom of the chamber, we expect our theoretical model to be widely relevant to the modeling of experiments on collective behavior of catalytic Janus swimmers.

Indeed, future experimental and theoretical work may explore pair interactions between Janus swimmers of different type, as well as higher order interactions between $N > 2$ colloids. Additionally, our setup for the study of pair interactions in 1D confinement may also be applicable to other types of swimmers, from self-propelled droplets propelled by Marangoni effects,[67] to light-driven swimmers propelled by critical demixing of the surrounding solution,[68] to biological swimmers such as bacteria or microalgae.[69,70] Finally, addressing the effect of shape anisotropy on pair interaction of active colloids is an interesting

Table 1. Summary of the different kind of interactions observed in this work..

1D interactions		2D interactions					
$Pt@SiO_2$	$Cu@SiO_2$	$Pt@SiO_2$ (encounter angles)			$Cu@SiO_2$ (encounter angles)		
		<90°	90°	>90°	<90°	90°	>90°
Steric interaction	Repulsive interaction	Steric interaction	Steric interaction	Steric interaction	Repulsive interaction	Repulsive interaction	Repulsive interaction

aspect that is worth investigation in a future contribution, both from a theoretical as well from an experimental standpoint.

4. Experimental Section

Preparation of $Pt@SiO_2$ and $Cu@SiO_2$ Janus Colloids: Janus colloids were obtained by drop casting a suspension of spherical SiO_2 (3 µm diameter, Sigma–Aldrich) particles in ethanol on a plasma cleaned glass slide, followed by slow evaporation of the solvent, to form a monolayer. Next, a thin layer of Pt was deposited using an e-beam system (or Cu was thermally evaporated in case of $Cu@SiO_2$) on the monolayer. Finally, the Janus colloids were released in de-ionized water by applying short ultrasonic pulses.

Preparation of Cracked SU8 Substrate: The SU8 coated substrate was prepared by following common photolithography methods and Kraft et al.[71] Briefly, photoresist SU8 was spin coated on a clean glass slide followed by soft baking, exposing to UV light and hard baking steps. Thermal stresses during baking result in the crack formation on SU8.

Motion Studies of $Pt@SiO_2$ and $Cu@SiO_2$ Particles on the Cracks (1D): Motion observations were performed on the cracks using an inverted microscope. Briefly, a 1 µL aqueous suspension of either $Pt@SiO_2$ or $Cu@SiO_2$ particles was placed on the SU8 coated glass slide (containing cracks). After allowing the particles to sediment for a few seconds, a 20 µL H_2O_2 solution (either 2.5 v/v% or 5 v/v%) was added. The motion of the particles was recorded in the cracks at 40 frames per second.

Motion Studies of $Pt@SiO_2$ and $Cu@SiO_2$ Particles Without any Confinement (2D): Motion studies were performed on a cleaned glass slide (cleaned with acetone, ethanol, followed by plasma treatment) by placing a 1 μL aqueous suspension of either $Pt@SiO_2$ or $Cu@SiO_2$ particles. After allowing particle sedimentation, a 20 μL H_2O_2 solution was added. The motion of the particles was recorded at 40 frames per second.

Video Recording and Speed Analysis: All the videos were recorded using a Zeiss camera (Axiocam 702 Mono) attached to a Carl Zeiss inverted microscope. The videos were analyzed using MATLAB to yield trajectories with $x - y$ coordinates which were further processed for calculating instantaneous speeds every frame using simple distance between two Cartesian coordinates formula. Finally, the tracks with the instantaneous speeds were plotted using MATLAB.

In-Plane and Zenith Angle Analysis: In-plane angle (ϕ) calculation was done in ImageJ and MATLAB following Wang et al.[72] Briefly, the center of the whole colloid and the metal coated part was determined using ImageJ after appropriate thresholding of the videos. Finally, the arctan of the two Cartesian coordinates obtained were processed in MATLAB, to yield in-plane angle values using the formula $(\phi) = \arctan(\frac{y_0 - y_1}{x_0 - x_1})$, where (x_0, y_0) are the coordinates of the center of the whole colloid and (x_1, y_1) of the metal part.

The zenith angle (θ) was evaluated every frame using ImageJ following Xiao et al.[73] Briefly, θ can be calculated using the formula $B = \frac{A}{2}(1 + \cos\theta)$, where, A is the brightness of the colloid when the θ is 0° and B is the brightness when θ is non-zero. The brightness (A or B) is obtained from ImageJ by multiplying the area of the colloid with the pixel intensity (or mean gray value), every frame.

Theory: As already mentioned in the main text, the swimming velocities can conveniently be decomposed into diffusiophoretic (D) and hydrodynamic (H) contributions as $V_i^{\xi} = V_{i,\mathrm{D}}^{\xi} + V_{i,\mathrm{H}}^{\xi}$ and $\boldsymbol{\Omega}_i^{\xi} = \boldsymbol{\Omega}_{i,\mathrm{D}}^{\xi} + \boldsymbol{\Omega}_{i,\mathrm{H}}^{\xi}$, where $\xi \in \{\mathrm{S}, \mathrm{P}\}$ with S and P denoting self and pair interactions, respectively. The velocities are expressed in terms of the small dimensionless parameters $\epsilon = a/h$ and $\delta = a/\ell$, with a denoting the particle radius, h the height above the wall, and ℓ the interparticle distance. For future reference, we define $u_i^{\parallel} = \hat{u}_i - (\hat{u}_i \cdot \hat{e}_z)\hat{e}_z$, denoting the projection of the orientation vector on a plan parallel to the substrate.

We first calculate the translational and angular velocities of a single particle in the presence of a wall. It follows from the reciprocal theorem in fluid mechanics [74] that the translation and rotational velocities of an active colloid are obtained as [56,75]

$$V_i^{\mathrm{S}} = -\langle \nu_i^{\mathrm{S}} \rangle, \qquad \boldsymbol{\Omega}_i^{\mathrm{S}} = \frac{3}{2a} \langle \nu_i^{\mathrm{S}} \times \hat{n}_i \rangle, \tag{4}$$

for $i \in \{1, 2\}$, with ν^{S} denoting the tangential slip velocity. Here, $\langle \cdot \rangle$ denotes the average operator over the surface of a sphere. The self-induced velocities of an active colloid near a wall have previously been obtained by Ibrahim and Liverpool.[58,66] Using the multipole expansion, they showed that the phoretic parts can be expanded as series in the parameter ϵ as

$$V_{i,\mathrm{D}}^{\mathrm{S}} = V_{0i}\,\hat{u}_i + \frac{\alpha_i^{(0)}\mu_i^{(0)}}{4D}\,\epsilon^2\,\hat{e}_z + \mathcal{O}(\epsilon^3), \tag{5a}$$

$$\boldsymbol{\Omega}_{i,\mathrm{D}}^{\mathrm{S}} = \frac{3\Lambda_i}{16aD}\,u_i^{\parallel} \times \hat{e}_z + \mathcal{O}(\epsilon^4), \tag{5b}$$

with

$$V_{0i} = -\frac{1}{15D}\left(5\alpha_i^{(1)}\mu_i^{(0)} + 2\alpha_i^{(2)}\mu_i^{(1)}\right) \tag{6}$$

denoting the bulk swimming velocity, that is, in the absence of the confining wall. Here, we have defined the abbreviation

$$\Lambda_i = \mu_i^{(1)}\left(\alpha_i^{(0)}\sin\theta_i - \frac{\epsilon}{8}\,\alpha_i^{(1)}\sin 2\theta_i\right)\epsilon^2\,. \tag{7}$$

In turn, the leading-order contribution to the hydrodynamic-induced velocities is given by

$$V_{i,\mathrm{H}}^{\mathrm{S}} = \frac{3\kappa_i}{16}\,\epsilon^2\left(\sigma_i^{\parallel}\hat{e}_i^{\parallel} + \sigma_i^{\perp}\hat{e}_z\right) + \mathcal{O}(\epsilon^3), \tag{8a}$$

$$\boldsymbol{\Omega}_{i,\mathrm{H}}^{\mathrm{S}} = -\frac{3\kappa_i}{32a}\,\epsilon^3\sigma_i^{\parallel}\hat{e}_i^{\parallel} \times \hat{e}_z + \mathcal{O}(\epsilon^4), \tag{8b}$$

with κ_i denoting the relevant polarity coefficients given by

$$\kappa_i = \frac{1}{4D}\left(\alpha_i^{(1)}\mu_i^{(1)} + 2\alpha_i^{(2)}\mu_i^{(0)}\right). \tag{9}$$

In addition, we have defined the shorthand notations $\sigma_i^{\parallel} = 2\sin 2\theta_i$ and $\sigma_i^{\perp} = (1 + 3\cos 2\theta_i)$ together with the abbreviation $\hat{e}_i^{\parallel} = (\cos\phi_i, \sin\phi_i, 0)^{\top}$ with $\top$ denoting the transpose operator. It follows that $u_i^{\parallel} = \sin\theta_i\,\hat{e}_i^{\parallel}$.

We note that the source-dipole and force-quadrupole lead to contributions that scale as ϵ^3 and ϵ^4 to the translational and angular velocities, respectively. Therefore, these have not been accounted for to the order of expansion considered here. These contributions involve the third moment of the activity profile, $\alpha^{(3)}$. We have checked that including these additional terms does not alter the resulting induced swimming velocities and rotation rates significantly.

Next, we calculate the translational and rotational velocities induced by the second particle. We define the unit vector connecting the two active particles, directed from particle 1 to 2, as $\hat{s}_{12} = (x_2 - x_1)/\ell$, where $\ell = |x_2 - x_1|$. We derive far-field expressions of the induced translational and rotational velocities resulting from pair interactions between two active colloids at arbitrary height above a no-slip wall. Then, the phoretic contribution to the drift velocities is obtained as

$$V^{\mathrm{P}}_{2,\mathrm{D}} = \frac{2\alpha^{(0)}_1 \mu^{(0)}_2}{D}\,\delta^2\,\hat{s}_{12} + \mathcal{O}(\delta^3), \tag{10a}$$

$$\boldsymbol{\Omega}^{\mathrm{P}}_{2,\mathrm{D}} = \frac{3\alpha^{(0)}_1 \mu^{(1)}_2}{2aD}\,\delta^2(\hat{u}_2 \times \hat{s}_{12} + \boldsymbol{\Gamma}_{12}) + \mathcal{O}(\delta^4), \tag{10b}$$

where

$$\boldsymbol{\Gamma}_{12} = (\delta/\epsilon)\Big(\big(1 - 3s_z^2\big)\hat{u}_2 \times \hat{e}_z + 3s_z\, s^{\parallel}_{12} \times \hat{u}_2\Big). \tag{11}$$

Here, we have defined the notation $s_\xi = \hat{s}_{12} \cdot \hat{e}_\xi$, with $\xi \in \{x, y, z\}$ and introduced, for convenience, the abbreviation $s^{\parallel}_{12} = \hat{s}_{12} - s_z\hat{e}_z$.

Lastly, the translational and rotational velocities resulting from dipolar hydrodynamic interactions induced by the second particle are obtained as

$$V^{\mathrm{P}}_{2,\mathrm{H}} = 6\kappa_1\,\delta^2\,\sin 2\theta_1\Big(\hat{s}_{12} \cdot \hat{e}^{\parallel}_1\Big)s_z\,\hat{s}_{12} + \mathcal{O}(\delta^3), \tag{12a}$$

$$\boldsymbol{\Omega}^{\mathrm{P}}_{2,\mathrm{H}} = 6(\kappa_1/a)\delta^3\,\sin 2\theta_1\,\boldsymbol{\omega}_1 + \mathcal{O}(\delta^4), \tag{12b}$$

where the dipole coefficient κ_1 has been defined by Equation (9) above. Here, we have defined

$$\boldsymbol{\omega}_1 = \begin{pmatrix} \big(s_z^2 - s_y^2\big)\sin\phi_1 - s_x s_y \cos\phi_1 \\ \big(s_x^2 - s_z^2\big)\cos\phi_1 + s_x s_y \sin\phi_1 \\ s_z\big(s_y\cos\phi_1 - s_x\sin\phi_1\big) \end{pmatrix}. \tag{13}$$

The sum of all these contributions to the translational and rotational velocities of each particle enter into the equations of motion (1), which become (2–3) when particularized to the 1D geometry. The lateral walls of the crack exert steric forces on the confined active colloids. In our simulations, we have simply assumed that the particles move solely along the direction of the crack. Introducing a confining potential along the lateral direction would lead to identical results.

Supporting Information

Supporting Information is available from the Wiley Online Library or from the author.

Acknowledgements

J.S. and P.S. acknowledge the Volkswagen foundation for financial support in form of a Freigeist grant (no. 91619) and the Fulbright Foundation for a Fulbright Cottrell award. The authors would also like to acknowledge Zuyao Xiao for the help with the MATLAB codes and Anish Das and Prof. Detlev Belder for fabricating SU8. The authors thank Viktoryia Novak for her assistance in preparing Figure 1. This work has received support from the Max Planck School Matter to Life and the MaxSynBio Consortium, which were jointly funded by the Federal Ministry of Education and Research (BMBF) of Germany, and the Max Planck Society.

Open Access funding enabled and organized by Projekt DEAL.

Conflict of Interest

The authors declare no conflict of interest.

Data Availability Statement

The data that support the findings of this study are available from the corresponding author upon reasonable request.

Keywords

active matter, diffusiophoresis, pair interactions

Received: January 29, 2023
Revised: March 16, 2023
Published online:

[1] G. Gompper, R. G. Winkler, T. Speck, A. Solon, C. Nardini, F. Peruani, H. Löwen, R. Golestanian, U. B. Kaupp, L. Alvarez, T. Ki⊘rboe, E. Lauga, W. C. K. Poon, A. DeSimone, S. Muiños-Landin, A. Fischer, N. A. Söker, F. Cichos, R. Kapral, P. Gaspard, M. Ripoll, F. Sagues, A. Doostmohammadi, J. M. Yeomans, I. S. Aranson, C. Bechinger, H. Stark, C. K. Hemelrijk, F.J. Nedelec, T. Sarkar, et al.*J. Phys.: Condens. Matter* **2020**, *32*, 193001.
[2] P. W. Anderson, *Science* **1972**, *177*, 393.
[3] R. Golestanian, T. B. Liverpool, A. Ajdari, *Phys. Rev. Lett.* **2005**, *94*, 220801.
[4] J. R. Howse, R. A. L. Jones, A. J. Ryan, T. Gough, R. Vafabakhsh, R. Golestanian, *Phys. Rev. Lett.* **2007**, *99*, 048102.
[5] S. Das, A. Garg, A. I. Campbell, J. Howse, A. Sen, D. Velegol, R. Golestanian, S. J. Ebbens.,*Nat. Commun.* **2015**, *6*, 8999.
[6] L. Feuerstein, C. G. Biermann, Z. Xiao, C. Holm, J. Simmchen, *J. Am. Chem. Soc.* **2021**, *143*, 17015.
[7] M. Wittmann, S. Heckel, F. Wurl, Z. Xiao, T. Gemming, T. Strassner, J. Simmchen, *Chem. Commun.* **2022**, *58*, 4052.
[8] M. Franzl, S. Mui.nos-Landin, V. Holubec, F. Cichos, *ACS Nano* **2021**, *15*, 3434.
[9] X.Wang,K. Chen, P.C.and Kroy, V. Holubec, F. Cichos, *Nat. Commun.* **2023**, *14*, 56.
[10] R. Niu, E. C. Oğuz, H. Müller, A. Reinmüller, D. Botin, H. Löwen, T. Palberg, *Phys. Chem. Chem. Phys.* **2017**, *19*, 3104.
[11] F. Ginot, J. Caspers, M. Krüger, C. Bechinger, *Phys. Rev. Lett.* **2022**, *128*, 028001.
[12] N. Möller, S. Seiffert, T. Palberg, R. Niu, *ChemNanoMat* **2021**, *7*, 1145.
[13] U. Khadka, V. Holubec, H. Yang, F. Cichos, *Nat. Commun.* **2018**, *9*, 1.
[14] F. A Lavergne, H. Wendehenne, T. Bäuerle, C. Bechinger, *Science* **2019**, *364*, 70.
[15] R. Golestanian, *Phys. Rev. Lett.* **2012**, *108*, 038303.
[16] H. Stark, *Acc. Chem. Res.* **2018**, *51*, 2681.
[17] S. Saha, R. Golestanian, S. Ramaswamy, *Phys. Rev. E* **2014**, *89*, 062316.
[18] J. A. Cohen, R. Golestanian, *Phys. Rev. Lett.* **2014**, *112*, 068302.
[19] C. Bechinger, R. Di Leonardo, H. Löwen, C. Reichhardt, G. Volpe, G. Volpe, *Rev. Mod. Phys.* **2016**, *88*, 045006.

[20] B. Liebchen, A. K. Mukhopadhyay, *J. Phys.: Condens. Matter* **2021**, *34*, 083002.
[21] J. Agudo-Canalejo, R. Golestanian, *Phys. Rev. Lett.* **2019**, *123*, 018101.
[22] J. Palacci, S. Sacanna, A. P. Steinberg, D. J. Pine, P. M. Chaikin, *Science* **2013**, *339*, 936.
[23] I. Theurkauff, C. Cottin-Bizonne, J. Palacci, C. Ybert, L. Bocquet, *Phys. Rev. Lett.* **2012**, *108*, 268303.
[24] I. Buttinoni, J. Bialkè, F. Kümmel, H. Löwen, C. Bechinger, T. Speck, *Phys. Rev. Lett.* **2013**, *110*, 238301.
[25] F. Ginot, I. Theurkauff, F. Detcheverry, C. Ybert, C. Cottin-Bizonne, *Nat. Commun.* **2018**, *9*, 1.
[26] S. Heckel, J. Grauer, M. Semmler, T. Gemming, H. Löwen, B. Liebchen, J. Simmchen, *Langmuir* **2020**, *36*, 12473.
[27] L. D. Renner, D. B. Weibel, *MRS Bull.* **2011**, *36*, 347.
[28] E. Crosato, L. Jiang, V. Lecheval, J. T. Lizier, X. R. Wang, P. Tichit, G. Theraulaz, M. Prokopenko, *Swarm Intell.* **2018**, *12*, 283.
[29] T. Feder, *Phys. Today* **2007**, *60*, 28.
[30] M. Ballerini, N. Cabibbo, R. Candelier, A. Cavagna, E. Cisbani, I. Giardina, V. Lecomte, A. Orlandi, G. Parisi, A. Procaccini, M. Viale, V. Zdravkovic, *Proc. Natl. Acad. Sci. U.S.A.* **2008**, *105*, 1232.
[31] J. L. Moran, J. D. Posner, *Ann. Rev. Fluid Mech.* **2017**, *49*, 511.
[32] R. Golestanian, Lecture Notes - Les Houches Summer School, **2019**.
[33] N. Sharifi-Mood, A. Mozaffari, U. M. Còrdova-Figueroa, *J. Fluid Mech.* **2016**, *798*, 910.
[34] A. Varma, T. D. Montenegro-Johnson, S. Michelin, *Soft Matter* **2018**, *14*, 7155.
[35] S. Saha, S. Ramaswamy, R. Golestanian, *New J. Phys.* **2019**, *21*, 063006.
[36] B. Nasouri, R. Golestanian, *Phys. Rev. Lett.* **2020**, *124*, 168003.
[37] B. Nasouri, R. Golestanian, *J. Fluid Mech.* **2020**, *905*, A13.
[38] R. Soto, R. Golestanian, *Phys. Rev. Lett.* **2014**, *112*, 068301.
[39] M. S. D. Wykes, J. Palacci, T. Adachi, L. Ristroph, X. Zhong, M. D. Ward, J. Zhang, M. J. Shelley, *Soft Matter* **2016**, *12*, 4584.
[40] E. L. Jewell, W. Wang, T. E. Mallouk, *Soft Matter* **2016**, *12*, 2501.
[41] A. Pandey, P. B. S. Kumar, R. Adhikari, *Soft Matter* **2016**, *12*, 9068.
[42] A. I. Campbell, S. J. Ebbens, P. Illien, R. Golestanian, *Nat.Commun.* **2019**, *10*, 1.
[43] R.D. Baker, T. Montenegro-Johnson, A.D. Sediako, M.J. Thomson, A. Sen, E. Lauga, I.S. Aranson, *Nat. Commun.* **2019**, *10*, 4932.
[44] J. Katuri, R. Poehnl, A. Sokolov, W. Uspal, A. Snezhko, *Sci.Adv.* **2022**, *8*, eabo3604.
[45] P. Sharan, Z. Xiao, V. Mancuso, W. E. Uspal, J. Simmchen, *ACS Nano* **2022**, *16*, 4599.
[46] Z. Xiao, A. Nsamela, B. Garlan, J. Simmchen, *Angew. Chem. Int. Ed.* **2022**, *61*, e202117768.
[47] J. Simmchen, V. Magdanz, S. Sanchez, S. Chokmaviroj, D. Ruiz-Molina, A. Baeza, O. G. Schmidt, *RSC Adv.* **2014**, *4*, 20334.
[48] J. Katuri, W. E. Uspal, J. Simmchen, A. Miguel-Lòpez, S. Sànchez, *Sci. Adv.* **2018**, *4*, eaao1755.
[49] L. Wang, A. Kaeppler, D. Fischer, J. Simmchen, *ACS Appl. Mater. Interfaces* **2019**, *11*, 32937.
[50] I. P. Madden, L. Wang, J. Simmchen, E. Luijten, *Small* **2022**, 2107023.
[51] J. Simmchen, J. Katuri, W. E. Uspal, M. N. Popescu, M. Tasinkevych, S. Sànchez, *Nat. Commun.* **2016**, *7*, 1.
[52] S. Ebbens, D. A. Gregory, G. Dunderdale, J. R. Howse, Y. Ibrahim, T. B. Liverpool, R. Golestanian, *Europhys. Lett.* **2014**, *106*, 58003.
[53] A. Brown, W. Poon, *Soft Matter* **2014**, *10*, 4016.
[54] X. Zhou, S. Wang, L. Xian, Y. Shah, Z. H.and Li, Y. Lin, G.and Gao.,*Phys. Rev. Lett.* **2021**, *127*, 168001.
[55] M. N. Popescu, W. E. Uspal, C. Bechinger, P. Fischer, *Nano Lett.* **2018**, *18*, 5345.
[56] R. Golestanian, T. B. Liverpool, A. Ajdari, *New J. Phys.* **2007**, *9*, 126.
[57] Z.H. Shah, L.and Zhou X. Wang, S.and Xian, Y. Chen, G. Lin, Y. Gao, *Chem. Commun.* **2020**, *56*, 15301.
[58] Y. Ibrahim, T. B. Liverpool, *Eur. Phys. J. Special Topics* **2016**, *225*, 1843.
[59] P. Malgaretti, M. N. Popescu, S. Dietrich, *Soft Matter* **2018**, *14*, 1375.
[60] A. Daddi-Moussa-Ider, B. Kaoui, H. Löwen, *J. Phys. Soc. Jpn.* **2019**, *88*, 054401.
[61] A. Daddi-Moussa-Ider, A. R. Sprenger, Y. Amarouchene, T. Salez, C. Schönecker, T. Richter, H. Löwen, A. M. Menzel, *J. Fluid Mech.* **2020**, *904*, A34.
[62] A. Daddi-Moussa-Ider, A. R. Sprenger, T. Richter, H. Löwen, A. M. Menzel, *Phys. Fluids* **2021**, *33*, 082011.
[63] A. Daddi-Moussa-Ider, A. Vilfan, R. Golestanian, *J. Fluid Mech.* **2022**, *940*, A12.
[64] J. L. Anderson, *Ann. Rev. Fluid Mech.* **1989**, *21*, 61.
[65] B. Liebchen, H. Löwen, *J. Chem. Phys.* **2019**, *150*, 061102.
[66] Y. Ibrahim, T. B. Liverpool, *Europhys. Lett.* **2015**, *111*, 48008.
[67] R. Seemann, J.-B. Fleury, C. C. Maass, *Eur. Phys. J. Special Topics* **2016**, *225*, 2227.
[68] I. Buttinoni, G. Volpe, F. Kümmel, G. Volpe, C. Bechinger, *J. Phys.: Condens. Matter* **2012**, *24*, 284129.
[69] M. Polin, I. Tuval, K. Drescher, J. P. Gollub, R. E. Goldstein, *Science* **2009**, *325*, 487.
[70] J. Schwarz-Linek, J. Arlt, A. Jepson, A. Dawson, T. Vissers, D. Miroli, T. Pilizota, V. A. Martinez, W. C. K. Poon, *Colloids Surf. B: Biointerfaces* **2016**, *137*, 2.
[71] B. Krafft, R. Panneerselvam, D. Geissler, D. Belder, *Anal. Bioanal. Chem.* **2020**, *412*, 267.
[72] X. Wang, M. In, C. Blanc, A. Würger, M. Nobili, A. Stocco, *Langmuir* **2017**, *33*, 13766.
[73] Z. Xiao, S. Duan, P. Xu, J. Cui, H. Zhang, W. Wang, *ACS nano* **2020**, *14*, 8658.
[74] H. Masoud, H. A. Stone, *J. Fluid Mech.* **2019**, 879.
[75] H. A. Stone, A. D. T. Samuel, *Phys. Rev. Lett.* **1996**, *77*, 4102.